

## Deformable 4DCT lung registration with vessel bifurcations

A. Hilsmann<sup>a</sup>, T. Vik<sup>a</sup>, M. Kaus<sup>a</sup>, K. Franks<sup>b</sup>, J.-P. Bissonette<sup>b</sup>, T. Purdie<sup>b</sup>, A. Beziak<sup>b</sup>,  
T. Aach<sup>c</sup>

<sup>a</sup>Philips Research Europe, Hamburg

<sup>b</sup>Princess Margaret Hosp., Toronto

<sup>c</sup>RWTH Aachen University

**Abstract.** In radiotherapy planning of lung cancer, breathing motion causes uncertainty in the determination of the target volume. Image registration makes it possible to get information about the deformation of the lung and the tumor movement in the respiratory cycle from a few images. A dedicated, automatic, landmark-based technique was developed that finds corresponding vessel bifurcations. Hereby, we developed criteria to characterize *pronounced* bifurcations for which correspondence finding was more stable and accurate. The bifurcations were extracted from automatically segmented vessel trees in maximum inhale and maximum exhale CT thorax data sets. To find corresponding bifurcations in both data sets we used the shape context approach of Belongie *et al.* Finally, a volumetric lung deformation was obtained using thin-plate spline interpolation and affine registration. The method is evaluated on 10 4D-CT data sets of patients with lung cancer.

*Keywords:* medical image processing, landmark-based elastic registration, lung registration, radiotherapy planning

---

### 1. Introduction

In radiotherapy planning one important aspect is to determine the target volume that is to be treated with radiation. Physiological movement of patient or organs, e.g. breathing motion, affects the definition of the target volume. In the context of lung tumor radiation planning respiratory models and the movement of tumors over the respiratory cycle are currently being investigated. Deformable image registration has the potential to reduce geometric uncertainty, and provides the opportunity to increase treatment accuracy and precision by optimizing treatment in response to anatomical changes. This may allow for dose escalation. In order to capture movements of the inner lung, landmark based registration with landmarks on the inner vessel tree of the lung seems to be most promising because the vessels fill out the entire lung. Automatic landmark localization is important for clinical applications, as manual selection is time-consuming and often inaccurate.

### 2. Methods

#### 2.1 Landmark extraction

Landmarks were extracted from the inner vessel tree of the lung. For vessel tree segmentation we used a front propagation algorithm [1], [2] that outputs a centerline representation of the vessel tree. The algorithm was extended to determine seed points automatically on the vessels. From the centerline we selected *pronounced* vessel bifurcations as landmarks. These bifurcations are formally defined as follows:

- The bifurcation consists of three vessel branches with radii  $r_i, i = 1,2,3$ .
- $1/m \sum r_i > \bar{R} - \sigma_R$  where  $\bar{R}$  and  $\sigma_R$  denote the average and standard deviation of all radii in the centerlines of the whole vessel tree.

- $\forall r_i : |r_i - \text{median}(r_i)| / \text{MAD}(r_i) < 2$  where  $\text{MAD}(r_i)$  is the median absolute deviation ( $\text{MAD}(X) = \text{median}|x_i - \text{median}(X)|$  with a population  $X = (x_1, x_2, \dots, x_n)$  of the radii of branches at that particular bifurcation.

Thereby we account for differences in parts of the vessel tree from one breathing state to the other that may cause segmentation differences in both images. Correspondence finding from those bifurcations was more stable and accurate than correspondence finding with all bifurcations.

## 2.2 Landmark matching

In order to define point correspondences in the lung we matched the vessel trees using features extracted from bifurcations. The 2D shape context as a regional shape descriptor was first introduced by Belongie *et al.* [3]. A 3D modification has already been applied to tree-like structures like the bronchial tree or coronal arteries with good results [1]. The basic idea of the shape context is that a shape is represented by a set of  $n$  points sampled from the contours on the shape [3]. Each of these points is characterized by its local adjacencies given by the  $n - 1$  vectors originating from it to all other sample points on the shape. These vectors express the entire shape distribution relative to the reference point. As the full set of vectors is too detailed the shape is described by a coarse histogram. For each landmark-bifurcation we compute a 3D spherical histogram [1] in which the number of the displacement vectors to all remaining centerline points are counted for each bin. This histogram forms the feature vector. Assume a set of points  $C = (c_1, c_2, \dots, c_n), c_i \in \mathfrak{R}^3, i = 1, \dots, n$  being centerline points from the vessel tree and a set of points  $P = (p_1, p_2, \dots, p_m) \subset C, m < n, p_i \in \mathfrak{R}^3$  being selected bifurcations of the vessel tree. For each bifurcation  $p_j$  we capture the local shape represented by all centerline points  $c_i$  as seen from that bifurcation in the 3D shape context. The displacement vectors  $d_i = p_j - c_i, d_i \in \mathfrak{R}^3$  from the reference bifurcation  $p_j$  to the remaining centerline points  $c_i$  are expressed in spherical coordinates  $d_i(r, \theta, \phi)$  and the number of displacement vectors is counted for each bin. Hereby, the angles  $\phi$  and  $\theta$  are quantized linearly and the radius  $r$  is quantized logarithmically making the descriptor more sensitive to positions of nearby sample points than to those far away. This histogram is said to be the shape context of the point  $p$ . We normalize the histogram and additionally weight each bin with its volume, i.e. we record the density instead of the frequency. Assuming we are given two point sets  $P = (p_1, p_2, \dots, p_m), p_i \in \mathfrak{R}^3, i = 1 \dots m$  and  $Q = (q_1, q_2, \dots, q_n), q_j \in \mathfrak{R}^3, j = 1 \dots m$  being bifurcations of the maximum inhale and maximum exhale vessel trees, the cost function that measures the cost of matching the points  $p_i$  and  $q_j$  is given by the  $\chi^2$ -distance:

$$d_{\chi^2}(p_i, q_j) = \frac{1}{2} \sum_{d=1}^D \frac{(h_{dp_i} - h_{dq_j})^2}{h_{dp_i} + h_{dq_j}} \quad (1)$$

Corresponding landmarks in the maximum inhale data set to the maximum exhale data set are determined by minimizing the cost function.

## 2.3 Transformation estimation

Having identified the corresponding landmarks we estimate a volumetric transformation  $u$  that maps the maximum exhale landmark set  $\{q_i\}$  onto the maximum inhale landmark set  $\{p_i\}$  ( $u(p_i) = q_i$ ). The transformation can be

- 1) an affine transformation that is determined by an least squares approach minimizing the quadratic error between the actual and estimated positions or

- 2) an elastic transformation using thin-plate spline interpolation between the irregularly distributed bifurcations [4].

## 2. Results

### 3.1 Data

4D-CT data sets with voxel dimensions of 0.98 x 0.98 x 2.5 mm (left-right/LR, anterior-posterior/AP, inferior-superior/IS) of ten patients with lung cancer were analyzed. Eighteen corresponding vessel bifurcations were manually determined by an experienced physician in both phases. These points are referred to as *ground truth* points in the following. The *ground truth* points were selected such that three points lie each in the regions LUL (left upper lung), Lling (left lingular), LLL (left lower lung), RUL (right upper lung), RML (right middle lung) and RLL (right lower lung).

### 3.2 Ground truth analysis

We applied the transformation estimated from the automatically extracted landmarks to the *ground truth* point set from the maximum exhale phase and its estimated positions in the maximum inhale phase were compared to the actual positions of the ground truth points. Ideally, the estimated position coincides with the actual position. The differences between these positions are referred to as *landmark discrepancies* in the following. The registration result is reported as  $\bar{d}_{gt} \pm \sigma_{d_{gt}}$  where  $\bar{d}_{gt}$  denotes the average of all landmark discrepancies and  $\sigma_{d_{gt}}$  is the standard deviation. The average absolute landmark discrepancies were reduced from  $1.3 \pm 1.13$  mm to  $1.06 \pm 0.95$  mm in LR-, from  $1.76 \pm 1.32$  mm to  $1.24 \pm 1.27$  mm in AP- and from  $4.39 \pm 5.03$  mm to  $1.86 \pm 1.94$  mm in IS-direction with thin-plate spline interpolation. The registration error using affine registration was  $1.224 \pm 1.69$  mm (LR),  $1.44 \pm 2.02$  mm (AP) and  $2.30 \pm 3.22$  mm (IS). The average Euclidean distance between the *ground truth* points was  $2.85 \pm 2.11$  mm for thin-plate spline interpolation and  $3.40 \pm 2.38$  mm for affine registration. A paired t-test showed that the alignment accuracy was significant in all six regions of the lung referred to the breathing motion (see Table 1). A second paired t-test showed that in the upper and middle lung the thin-plate spline interpolation performance is significantly better than the performance of an affine registration (see Table 1). In the lower lung where the deformation is largest both transformations do not differ significantly.

Table 1  
Paired t-tests with 29 degrees of freedom.

regions	one-sided paired t-test		two-sided paired t-test	
	align. accuracy – magn. of motion		affine reg. – thin-plate splines	
	t-value	p-value	t-value	p-value
LUL	1.89	0.03500	2.13	0.02100
Lling	3.03	0.00260	2.08	0.02400
LLL	6.72	0.00005	0.18	0.43000
RUL	1.51	0.07100	3.53	0.00070
RML	3.31	0.00200	2.59	0.00740
RLL	6.75	0.00050	1.49	0.07403

### 3.2 Difference images

The second validation method relies on the difference images before and after registration. We transform the maximum inhale image on the maximum exhale image

by applying the transformation estimated from the automatically extracted landmarks backwardly. We obtain a transformed version of the inhale image that, in the ideal case, is equal to the exhale image. Comparing the difference images before and after registration provides us with information about the registration result that depends on the image information only. Figure 1 presents an example of difference images in the axial and the sagittal plane. From the observation of the difference images it becomes obvious that the differences between the images are reduced near the vessels and the tumor and furthermore near the diaphragm.

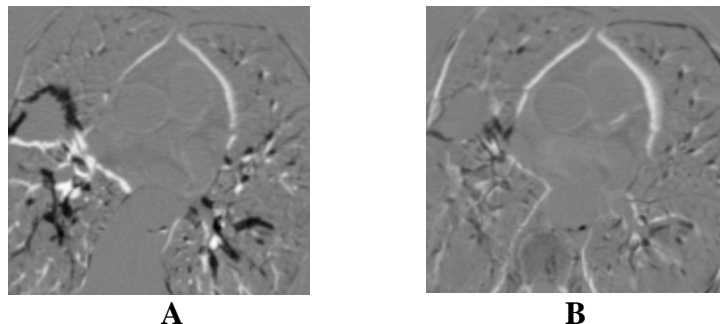


Fig. 1. Difference images in the axial plane before (A) and after (B) registration

#### 4. Discussion and conclusion

In order to assess breathing motion information, a landmark-based registration technique with automatically extracted *pronounced* vessel bifurcations was developed. The average resulting registration error was  $2.85 \pm 2.11$  mm for thin-plate spline and  $3.40 \pm 2.38$  mm for affine registration. Referring to other landmark-based lung registration methods, Urschler *et al.* [5] used point correspondences from lung and diaphragm surfaces for a thin-plate spline registration and achieved mean registration errors in the range of 5 to 9 mm in experiments on CT sheep scans with voxel dimensions of 0.5 mm x 0.52 mm x 0.6 mm. Coselmon *et al.* [6] applied gray value based image registration using mutual information and thin-plate spline interpolation. They achieved an alignment accuracy of 1.7 mm, 3.1 mm and 3.6 mm in the LR-, AP- and IS-directions. Compared to these registration results we obtain smaller registration errors despite lower image resolution. Visual inspection of the difference images showed that the method performs well near the vessels and the tumor as well as in regions near the diaphragm.

#### References

- [1] T. Bülow, C. Lorenz and S. Renisch. A General Framework for Tree Segmentation and Reconstruction from Medical Volume Data. In: MICCAI 2004 (1), pp. 533-540.
- [2] T. Bülow, C. Lorenz, R. Wiemker and J. Honko. Point Based Methods for Automatic Bronchial Tree Matching and Labelling. In: Proc. of SPIE, Medical Imaging 2006, vol. 6143, March 2006.
- [3] S. Belongie, J. Malik and J. Puzicha. Matching Shapes. 8<sup>th</sup> Int. Conf. on Computer Vision, 1, pp. 454-463, 2001.
- [4] F.L. Bookstein. Principal Warps: Thin-Plate Splines and the Decomposition of Deformations. IEEE Transactions on Pattern Analysis and Machine Intelligence, 11(6), pp. 567-585, June 1989.
- [5] M. Urschler and H. Bischof. Assessing Breathing Motion by Shape Matching of Lung and Diaphragm Surfaces. In: Proceedings of SPIE Int. Opt. Eng., vol. 5746, pp. 440-452, April 2005.
- [6] M.M. Coselmon, J.M. Balter, D.L. Mc Shan and M.L. Kessler. Mutual Information Based CT Registration of the Lung at Exhale and Inhale Breathing States using Thin-Plate Splines. Medical Physics, 31(11), pp. 2942-2948, November 2004.